

Using Absorption Imaging to Study Ion Dynamics in an Ultracold Neutral Plasma

C. E. Simien, Y. C. Chen, P. Gupta, S. Laha, Y. N. Martinez, P. G. Mickelson, S. B. Nagel, and T. C. Killian
Rice University, Department of Physics and Astronomy and Rice Quantum Institute, Houston, Texas, 77251

(Dated: March 18, 2022)

We report optical absorption imaging of ultracold neutral plasmas. Images are used to measure the ion absorption spectrum, which is Doppler-broadened. Through the spectral width, we monitor ion equilibration in the first 250 ns after plasma formation. The equilibration leaves ions on the border between the weakly coupled gaseous and strongly coupled liquid states. On a longer timescale of microseconds, we observe radial acceleration of ions resulting from pressure exerted by the trapped electron gas.

Plasma physics traditionally studies systems with temperatures of thousands of kelvin or greater because collisional ionization of atoms requires kinetic energies on this scale. Ultracold neutral plasmas, created by photoionizing laser-cooled and trapped atoms, access an exotic regime in which particle energies can be on the order of 1 K.

Fundamental interest in ultracold neutral plasmas stems from a range of phenomena in the ultracold regime. Recent experiments have studied plasma creation [1], collective modes [2], and recombination into highly excited Rydberg atomic states [3]. The spontaneous evolution of a dense, ultracold gas of Rydberg atoms into an ultracold plasma has also been investigated [4]. This is part of a search in atomic clouds for an analog of the Mott insulator-conductor transition in condensed matter [5]. Recombination in these systems resembles the methods used to produce cold antihydrogen with trapped positrons and antiprotons [6, 7].

A series of theory papers [8, 9, 10, 11, 12] explored issues surrounding thermalization and recombination in ultracold neutral plasmas when both electrons and ions are near or in the strongly coupled regime [13]. In strongly coupled plasmas the electrical interaction energy between the charged particles exceeds the average kinetic energy. This reverses the traditional energy hierarchy that underlies our normal understanding of plasmas based on concepts such as Debye screening and hydrodynamics. Strongly coupled plasmas exist in dense astrophysical systems [14], matter irradiated with intense laser fields [15, 16], dusty plasmas of highly charged macroscopic particles [17], and non-neutral trapped ion plasmas [18] that are laser cooled until they freeze into Wigner crystals.

We now report the first results with a new probe of ultracold plasmas: absorption imaging. This technique provides *in situ*, non destructive measurements, and offers excellent spatial, temporal, and spectral resolution. We describe the use of this probe to study ion-ion equilibration and expansion of the plasma during the first few microseconds after photoionization, but we emphasize its great potential to study a host of phenomena such as ion collective modes [19], shock waves [11], recombination, and particle-particle spatial correlations [18].

The production of an ultracold neutral plasma starts with atoms that are cooled and confined in a magneto-

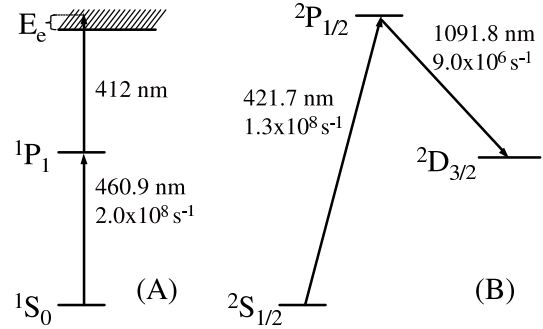


FIG. 1: Atomic and ionic energy levels involved in the experiment, with decay rates. (A) Neutral atoms are laser cooled and trapped in a magneto-optical trap (MOT) operating on the $1S_0 - 1P_1$ transition at 461 nm. Atoms excited to the $1P_1$ level by the MOT lasers are ionized by photons from a laser at ~ 412 nm. (B) Ions are imaged using the $2S_{1/2} - 2P_{1/2}$ transition at 422 nm. $2P_{1/2}$ ions decay to the $2D_{3/2}$ state 7% of the time, after which they cease to interact with the imaging beam. This does not complicate the experiment because ions typically scatter fewer than one photon during the time the imaging beam is on.

optical trap (MOT) (Fig. 1A). This aspect of the experiment was described in [20]. The neutral atom cloud is characterized by a temperature of about 20 mK and a density distribution given by $n(r) = n_0 \exp(-r^2/2\sigma^2)$, with $\sigma = 1$ mm and $n_0 = (4 \pm 2) \times 10^{10} \text{ cm}^{-3}$. The number of trapped atoms is $(6 \pm 1) \times 10^8$.

To form the plasma, the MOT magnets are turned off and atoms are ionized with photons from a 10 ns pulsed dye laser whose wavelength is tuned just above the ionization continuum (Fig. 1A). Because of the small electron-to-ion mass ratio, the initial electron kinetic energy (E_e) approximately equals the difference between the photon energy and the ionization potential. E_e/k_B can be as low as the bandwidth of the ionizing laser, which is ~ 100 mK. The initial kinetic energy for the resulting singly-charged, electronic ground state ions is close to that of the original neutral atoms. As we will discuss below, the resulting non-equilibrium plasma evolves rapidly. Up to $12 \pm 1\%$ of the neutral atoms are ionized producing plasmas with a peak density of $(5 \pm 3) \times 10^9 \text{ cm}^{-3}$.

Immediately after photoionization, the charge distribution is neutral everywhere. Due to the kinetic en-

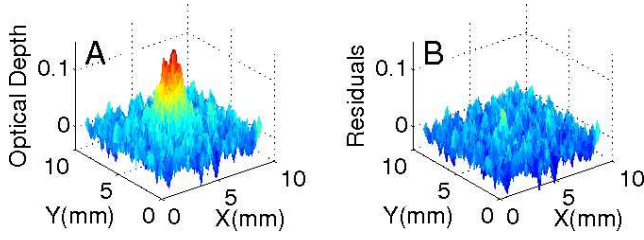


FIG. 2: Optical depth of an ultracold neutral plasma. (A) The delay between the formation of the plasma and image exposure is 100 ns, and the initial peak density is $n_{0i} = 5 \times 10^9 \text{ cm}^{-3}$. (B) Residuals of a fit to a two-dimensional Gaussian profile are close to the photon shot-noise.

ergy of the electrons, the electron cloud expands on the timescale of the inverse electron plasma frequency $\tau_e = \omega_{pe}^{-1} = \sqrt{m_e \epsilon_0 / n_e e^2} < 1 \text{ ns}$, where m_e , n_e , and e are the electron mass, density and charge. On this timescale the ions are essentially immobile. The resulting local charge imbalance creates a Coulomb potential energy well that traps all but a small fraction ($< 5\%$) of the electrons. Simulations [1] show that electrons escape mostly from the edges of the spatial distribution, and the center of the cloud is well described as a neutral plasma [21]. The diagnostic used in previous experiments was charged particle detection of electrons and ions after they had left the plasma.

Spectroscopic diagnostics are ubiquitous in plasma experiments, and some even provide spatial information, such as spatially resolved laser induced fluorescence [18, 22]. The absorption imaging reported here is particularly well-adapted for small, cold, relatively dilute plasmas that evolve very quickly. It is also a powerful technique for studying laser cooled and trapped neutral atoms [23]. A collimated laser beam, tuned near resonance with the principle transition in the ions (Fig. 1B), illuminates the plasma and falls on an image intensified CCD camera. Following Beer's law, the optical depth (OD) is defined in terms of the image intensity without ($I_{background}$) and with (I_{plasma}) the plasma present,

$$\begin{aligned} OD(x, y) &= \ln(I_{background}(x, y) / I_{plasma}(x, y)) \\ &= \alpha(\nu) \int_{-\infty}^{\infty} dz n_i(x, y, z), \\ &= \frac{n_{0i} \alpha(\nu)}{\sqrt{2\pi} \sigma_z} e^{-x^2/2\sigma_x^2 - y^2/2\sigma_y^2} \end{aligned} \quad (1)$$

where n_{0i} is the peak ion density, and $\alpha(\nu)$ is the absorption cross section at the image beam frequency, ν . In the last line we have inserted a Gaussian density distribution for the ions, which leads to the function used to fit the data.

Figure 2 shows a typical absorption image. The intensity of the probe beam is approximately $200 \mu\text{W}/\text{cm}^2$, which is much less than the saturation intensity of the transition ($38 \text{ mW}/\text{cm}^2$). The spatial resolution of typical images is about $100 \mu\text{m}$, limited by pixel averaging

performed to improve the signal-to-noise ratio of the images.

To study the time-evolution of the plasma, we vary the delay between the formation of the plasma and image exposure (t_{delay}) with 10 ns accuracy. The minimum camera exposure gate width is 50 ns. For the shortest exposure times, which we use for the best time resolution at very short t_{delay} , we typically average about 60 ionizing laser shots. For longer delay times we use longer image exposure times of up to 800 ns, and decrease the number of accumulations to keep the total number of photons detected approximately constant. The repetition rate for ionization and image recording is about 5 times per second.

The imaging beam itself can also be gated with a minimum width of about 200 ns. We use this capability for $t_{delay} > 1 \mu\text{s}$ to turn off the image beam until the camera exposure begins. This prevents optical pumping of the ions to the $^2D_{3/2}$ state (Fig. 1B).

Plotting the peak optical depth as a function of image laser frequency provides the absorption spectrum of the ions (Fig. 3). The imaging laser linewidth of about 5 MHz is negligible on the scale of the 21.5 MHz natural linewidth of the transition. As described below, additional broadening of the absorption spectrum provides a wealth of information on the plasma dynamics.

Here we describe experiments using the time evolution of the absorption spectrum to study ion dynamics for a plasma with $N_i = 7 \times 10^7$ ions, initial peak density for ions and electrons of $n_{0i} \approx n_{0e} = (5 \pm 3) \times 10^9 \text{ cm}^{-3}$, and $E_e/k_B = (68 \pm 5) \text{ K}$. We chose a relatively large E_e in order to avoid complications that arise when the electron Coulomb coupling parameter ($\Gamma_e = e^2/4\pi\epsilon_0 a k_B T_e$) approaches or initially exceeds unity, such as screening of the ion interaction [24], and rapid collisional recom-

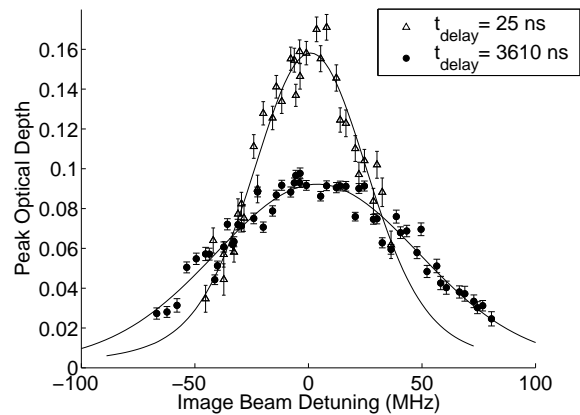


FIG. 3: Absorption spectra of ultracold neutral plasmas. We plot the peak optical depth derived from fits to data such as Fig. 2. The frequency is with respect to a Doppler-free absorption feature in a strontium discharge cell. Both spectra correspond to $E_e/k_B = 68 \text{ K}$ and the same initial peak plasma density of $n_{0i} = 5 \times 10^9 \text{ cm}^{-3}$. Data are fit with Voigt profiles, and the increase in linewidth for longer t_{delay} is clear.

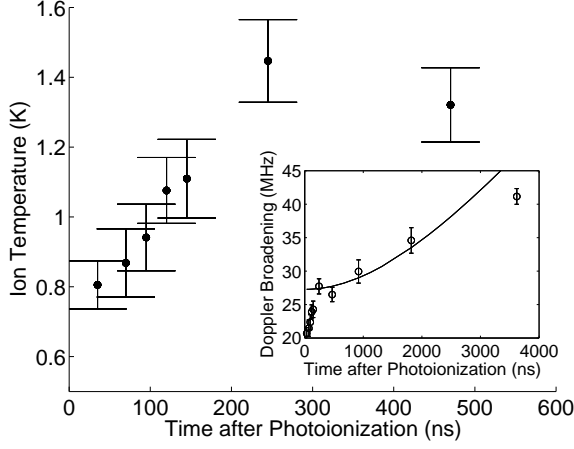


FIG. 4: Ion dynamics determined from the spectral width. Error bars are two sigma uncertainties from Voigt profile fits to absorption spectra. The time after photoionization corresponds to the timing of the center of the camera exposure gate. Data show disorder-induced heating of the ions as they equilibrate during $t_{delay} < 250$ ns. (Inset) For longer times, the Doppler broadening of the spectrum continues to increase as ions accelerate radially due to electron pressure. This process is described by a hydrodynamic model with no free parameters.

bination and heating of the electrons [9, 10, 11, 12]. Here, $a = (4\pi n_0 e / 3)^{-1/3}$ is the Wigner-Seitz radius, and $T_e = \frac{2}{3} E_e / k_B$ is the electron temperature as set by the wavelength of the ionizing laser. For this sample $\Gamma_e = 0.1$.

The observed spectral linewidths are all significantly broader than the natural linewidth of the transition. Collisional broadening is not significant because of the relatively low particle density and collision frequency in the sample. The dominant contribution to the linewidth is Doppler broadening, which makes the spectrum a very accurate probe of the ion velocity distribution. From the fit of each spectrum to a Voigt profile, we extract the rms Doppler broadening, $\sigma_D = \frac{\sqrt{k_B T_i / m_i}}{\lambda}$, where m_i is the ion mass, and λ is the wavelength of the transition. This allows us to determine an ion temperature (T_i) as a function of time, as shown in Fig. 4.

The temperature increases rapidly for $t_{delay} < 250$ ns. Two pieces of information imply that this is thermalization of ions with themselves after creation in a spatially disordered state. The timescale is on the order of the inverse plasma frequency of ions, $\tau_i = \omega_{pi}^{-1} = \sqrt{m_i \epsilon_0 / n_0 e^2} = 100$ ns, which is the timescale on which ions respond to perturbations from their equilibrium spatial distribution. The temperature of 1.4 ± 0.1 K derived from the Doppler width at 250 ns is also on the order of the amount of potential energy inherent in the initial disorder of the ions. A simple estimate implies there is $e^2 / 4\pi \epsilon_0 a k_B \approx 5$ K of potential energy that will be redistributed during thermalization.

This thermalization has been modelled with molecu-

lar dynamics simulations [8, 9, 10], and the experimental data is in general agreement with the theory. The accuracy of the imaging probe will enable detailed comparison of measurement and theory for the time dependence of the ion temperature.

The final temperature reached, however, can be compared with an expression derived in [8]. Assuming complete initial disorder and incorporating the screening effects of the electrons,

$$T_i = \frac{2}{3} \frac{e^2}{4\pi \epsilon_0 a k_B} \left| \tilde{U} + \frac{\kappa}{2} \right|. \quad (2)$$

Here, $\kappa = a / \lambda_D = \sqrt{3\Gamma_e} = 0.55$ where $\lambda_D = (\epsilon_0 k_B T_e / n_0 e^2)^{1/2} = 7 \mu\text{m}$ is the Debye length. The quantity $\tilde{U} \equiv \frac{U}{N_i e^2 / 4\pi \epsilon_0 a}$ is the potential energy per particle in units of $e^2 / 4\pi \epsilon_0 a$. It has been studied with molecular dynamics simulations [24] for a homogeneous system of particles interacting through a Yukawa potential, $\phi(r) = \frac{e^2}{4\pi \epsilon_0 r} \exp(-r / \lambda_D)$, which describes ions in the background of weakly coupled electrons [25]. The experimental values for n_i , T_i , and κ , imply $\tilde{U} = -0.73$. Equation 2 then gives $T_i = 1.4$ K, in excellent agreement with the measured value.

We now address the level of Coulomb coupling for the ions. From the temperature and peak density we derive $\Gamma_i = 3 \pm 1$ for the thermalized ion cloud at $t_{delay} = 250$ ns. For a system of charges embedded in a uniform neutralizing background, formally called a one-component plasma [26], local spatial correlations characteristic of a strongly coupled fluid appear for $\Gamma \geq 2$. For Debye shielded particles, such as the ions studied here, screening will reduce the correlations. This effect is approximately incorporated by using the effective coupling constant $\Gamma^* = \Gamma e^{-\kappa}$ [9, 24]. At 250 ns, $\Gamma_i^* = 2 \pm 1$, and the ions are just on the edge of the strongly coupled fluid phase. Perhaps other initial experimental parameters, or laser cooling of the ions [9, 27], will lead to more strongly coupled systems, although $\Gamma_i^* = 2$ already puts the experiment in an interesting regime.

For $t_{delay} > 250$ ns, the spectral width continues to increase, but at a slower rate, as shown in the inset of Fig. 4. This slow increase is due to outward radial acceleration of the ions caused by pressure exerted by the gas of trapped electrons. This was studied experimentally in [2] and theoretically by a variety of means in [11]. The experiments measured the final velocity that the ions acquired, which was approximately $\sqrt{E_e / m_i}$. Here we observe the ion dynamics at much earlier times during the acceleration phase.

A hydrodynamic treatment [2] predicts that the force per ion is

$$\bar{F} = \frac{\bar{\nabla}(n_e(r) k_B T_e)}{n_i(r)} = \hat{r} \frac{r k_B T_e}{\sigma_i^2}, \quad (3)$$

where the ion and electron density distributions are $n_e(r) \approx n_i(r) = n_0 \exp(-r^2 / 2\sigma_i^2)$. We approximate the

rms size (σ_i) as the mean of the observed sizes σ_x and σ_y , and we assume thermal equilibrium for the electrons throughout the cloud [11]. This force leads to a radial expansion velocity for the ions, $v_r(r)$, which is correlated with position and increases linearly with time. This does not represent an increase in the random thermal velocity spread or temperature of the ions. Due to the large mass difference, thermalization of ions and electrons [9] is slow and occurs on a millisecond timescale. The increase in Doppler broadening due to thermalization is approximately one order of magnitude smaller than what is observed.

Using the dynamics implied by Eq. 3, the evolution of the Doppler broadening can be calculated. The mean squared velocity component along the imaging laser is

$$\langle v_z^2 \rangle = \int d^3r dv_T \frac{n_i(r)}{N_i} P(v_T) (v_T + v_r(r) \cos \theta)^2, \quad (4)$$

where $P(v_T)$ is the thermal distribution of v_z for $T_i = 1.4$ K. The resulting theoretical Doppler broadening $\sqrt{\langle v_z^2 \rangle}/\lambda$, plotted in Fig. 4, reproduces the data accurately.

The ion acceleration is thus an excellent diagnostic of the electron temperature. This will be of great value in future studies because the temperature is predicted to evolve in a complicated fashion for lower initial Γ_e due to recombination and disorder-induced heating of the electrons [9, 10, 11, 12]. One also expects that there will be a cooling effect at longer t_{delay} due to expansion of the plasma and evaporative cooling [11]. The small

discrepancy between theory and data for long t_{delay} in Fig. 4 may indicate the onset of this cooling, although expansion of the plasma is small on the timescale of these observations. For the maximum t_{delay} and typical $v_r \approx 15$ m/s, $v_r t_{\text{delay}} \approx 50 \mu\text{m}$. This small increase in size is observed in the images (Fig. 2).

The initial study using absorption imaging of an ultracold neutral plasma has probed ion dynamics in the first few microseconds after photoionization. It revealed disorder-induced heating that was predicted in [8], and showed that the ions equilibrate on the boundary of the gas-liquid transition. Acceleration of ions due to electron pressure was also evident, and can be used to monitor the electron temperature.

Many future experiments suggest themselves. Some of the most interesting are investigating dynamics when the initial electron Coulomb coupling parameter is large and recombination and disorder-induced electron heating are expected to dominate the plasma evolution. Detailed study of ion and electron thermalization at the border of the strongly coupled regime is also possible. Improvements in the imaging optics will significantly increase the image signal-to-noise ratio and allow study of features on the ion density distribution with $\sim 10 \mu\text{m}$ experimental resolution.

This research was supported by the Department of Energy Office of Fusion Energy Sciences, Office for Naval Research, Research Corporation, Alfred P. Sloan Foundation, and David and Lucille Packard Foundation.

-
- [1] T. C. Killian, S. Kulin, S. D. Bergeson, L. A. Orozco, C. Orzel, and S. L. Rolston, *Phys. Rev. Lett.* **83**, 4776 (1999).
 - [2] S. Kulin, T. C. Killian, S. D. Bergeson, and S. L. Rolston, *Phys. Rev. Lett.* **85**, 318 (2000).
 - [3] T. C. Killian, M. J. Lim, S. Kulin, R. Dumke, S. D. Bergeson, and S. L. Rolston, *Phys. Rev. Lett.* **86**, 3759 (2001).
 - [4] M. P. Robinson, B. L. Tolra, M. W. Noel, T. F. Gallagher, and P. Pillet, *Phys. Rev. Lett.* **85**, 4466 (2000).
 - [5] G. Vitrant, J. M. Raimond, M. Gross, and S. Haroche, *J. Phys. B* **15**, 49 (1982).
 - [6] M. Amoretti et al., *Nature* **419**, 456 (2002).
 - [7] G. Gabrielse et al., *Phys. Rev. Lett.* **89**, 213401 (2002).
 - [8] M. S. Murillo, *Phys. Rev. Lett.* **87**, 115003 (2001).
 - [9] S. G. Kluzmin and T. M. O'Neil, *Phys. Plasmas* **9**, 3743 (2002).
 - [10] S. Mazevet, L. A. Collins, and J. D. Kress, *Phys. Rev. Lett.* **88**, 55001 (2002).
 - [11] F. Robicheaux and J. D. Hanson, *Phys. Plasmas* **10**, 2217 (2003).
 - [12] A. N. Tkachev and S. I. Yakovlenko, *Quantum Electronics* **30**, 1077 (2000).
 - [13] S. Ichimaru, *Rev. Mod. Phys.* **54**, 1017 (1982).
 - [14] H. M. V. Horn, *Science* **252**, 384 (1991).
 - [15] M. Nantel, G. Ma, S. Gu, C. Y. Cote, J. Itatani, and D. Umstadter, *Phys. Rev. Lett.* **80**, 4442 (1998).
 - [16] E. Springate, N. Hay, J. W. G. Tisch, M. B. Mason, T. Ditmire, M. H. R. Hutchinson, and J. P. Marangos, *Phys. Rev. A* **61**, 063201 (2000).
 - [17] G. E. Morfill, H. M. Thomas, U. Konopka, and M. Zuzic, *Phys. Plasmas* **6**, 1769 (1999).
 - [18] T. B. Mitchell, J. J. Bollinger, X. P. Huang, W. M. Itano, and D. H. E. Dubin, *Phys. Plasmas* **6**, 1751 (1999).
 - [19] M. S. Murillo, *Phys. Rev. Lett.* **85**, 2514 (2000).
 - [20] S. B. Nagel, C. E. Simien, S. Laha, P. Gupta, V. S. Ashoka, and T. C. Killian, *Phys. Rev. A* **67**, 011401 (2003).
 - [21] The approximate excess ion density is $3n_e(\lambda_D/\sigma)^2 \ll n_e$, where λ_D is the Debye screening length.
 - [22] F. M. Levinton and F. Trintchouk, *Rev. Sci. Instruments* **72**, 898 (2001).
 - [23] H. J. Metcalf and P. van der Straten, *Laser Cooling and Trapping* (Springer-Verlag New York, New York, 1999).
 - [24] R. T. Farouki and S. Hamaguchi, *J. Chem. Phys.* **101**, 9885 (1994).
 - [25] There are many electrons per Debye sphere ($\kappa^{-3} = n_e 4\pi\lambda_D^3/3 = 6$), which justifies the use of this model.
 - [26] D. H. E. Dubin and T. M. O. Neil, *Rev. Mod. Phys.* **71**, 87 (1999).
 - [27] T. C. Killian, V. S. Ashoka, P. Gupta, S. Laha, S. B. Nagel, C. E. Simien, S. Kulin, S. L. Rolston, and S. D.

Bergeson, *J. Phys. A: Math. Gen.* **36**, 6077 (2003).